

Force Matching with Relativistic Constraints: A Physics-Inspired Approach to Stable and Efficient Generative Modeling

Yang Cao* Bo Chen† Xiaoyu Li‡ Yingyu Liang§ Zhizhou Sha¶
 Zhenmei Shi|| Zhao Song** Mingda Wan††

Abstract

This paper introduces Force Matching (ForM), a novel framework for generative modeling that represents an initial exploration into leveraging special relativistic mechanics to enhance the stability of the sampling process. By incorporating the Lorentz factor, ForM imposes a velocity constraint, ensuring that sample velocities remain bounded within a constant limit. This constraint serves as a fundamental mechanism for stabilizing the generative dynamics, leading to a more robust and controlled sampling process. We provide a rigorous theoretical analysis demonstrating that the velocity constraint is preserved throughout the sampling procedure within the ForM framework. To validate the effectiveness of our approach, we conduct extensive empirical evaluations. On the *half-moons* dataset, ForM significantly outperforms baseline methods, achieving the lowest Euclidean distance loss of **0.714**, in contrast to vanilla first-order flow matching (5.853) and first- and second-order flow matching (5.793). Additionally, we perform an ablation study to further investigate the impact of our velocity constraint, reaffirming the superiority of ForM in stabilizing the generative process. The theoretical guarantees and empirical results underscore the potential of integrating special relativity principles into generative modeling. Our findings suggest that ForM provides a promising pathway toward achieving stable, efficient, and flexible generative processes. This work lays the foundation for future advancements in high-dimensional generative modeling, opening new avenues for the application of physical principles in machine learning.

* ycao4@wyomingseminary.org. Wyoming Seminary

† bc7b@mtmail.mtsu.edu. Middle Tennessee State University.

‡ xli216@stevens.edu. Stevens Institute of Technology.

§ yingyu@hku.hk. The University of Hong Kong. yliang@cs.wisc.edu. University of Wisconsin-Madison.

¶ shazz20@mails.tsinghua.edu.cn. Tsinghua University.

|| zhmeishi@cs.wisc.edu. University of Wisconsin-Madison.

** magic.linuxkde@gmail.com. Simons Institute for the Theory of Computing, University of California, Berkeley.

†† dylan.r.mathison@gmail.com. Anhui University.

Contents

1	Introduction	2
2	Related work	3
3	Preliminary	4
3.1	Notations	4
3.2	Flow Matching	4
3.3	Background on Special Relativity	5
4	Force Matching	6
4.1	Definition of Force Matching Objective	6
4.2	Our Result I: Sampling ODE	7
4.3	Our Result II: Speed Limit	7
4.4	Our Result III: ForM with TrigFlow	7
5	Experiment	8
5.1	Experiment setup	9
5.2	Results analysis	11
5.3	Euclidean distance loss	14
6	Empirical Ablation Study	14
7	Discussion	14
8	Conclusion	15
A	Theoretical Analysis	21
A.1	Sampling ODE	21
A.2	Speed Limit	23
A.3	ForM with TrigFlow	24
A.4	Relativistic Force Property	24

1 Introduction

The field of generative modeling has witnessed significant progress with the advent of sophisticated techniques that leverage neural networks to synthesize high-quality data. Recent methods such as Diffusion Models (DM) [SDWMG15, HJA20a, DN21, RBL⁺22, ZLCZ23, ZLKE23], Flow Matching (FM) [LCBH⁺22, LGL22, EKB⁺24], and the more recent Equilibrium Dynamics Model (EDM) [KAAL22, KAL⁺24] have emerged as prominent approaches, each exploring distinct generative paradigms. These techniques differ fundamentally in how they utilize neural networks to evolve data representations over time: while Diffusion Models rely on iterative transformations of a Gaussian-initialized distribution, EDM employs an Ordinary Differential Equation (ODE) for continuous evolution, and FM directly predicts the data’s velocity using a neural-network-based velocity field. Such diversity in generative approaches has motivated the need for a unified perspective that can bridge these conceptual differences.

In pursuit of this unification, TrigFlow [LS24] was proposed as a generalized framework that provides a continuous generative process capable of transitioning between the behaviors of EDM and FM. By leveraging trigonometric parameterization, TrigFlow formulates data generation through a combination of trigonometric components, allowing for a flexible representation that captures the strengths of both paradigms. The framework introduces a trigonometric-based parameterization of the generative process, a loss function aligning with diffusion methods, and a probability flow ODE, thereby offering a more comprehensive understanding of generative modeling techniques and providing a foundation for further advancements in this domain.

Building on this unification perspective, this paper introduces Force Matching (ForM) as a novel generative framework inspired by principles of relativistic mechanics to stabilize the sampling process. By incorporating relativistic constraints through the Lorentz factor, ForM ensures stable sampling dynamics, limiting the velocity of generated samples to avoid instability. We establish that ForM is well-aligned with consistency models, suggesting its potential to enhance scalable generative modeling solutions. Our contributions can be summarized as follows:

- We propose **Force Matching (ForM)**, a novel generative modeling framework inspired by relativistic mechanics, which ensures stable sampling by constraining sample velocities through the Lorentz factor.
- We establish theoretical foundations for ForM, highlighting its flexibility and scalability.
- We conduct extensive empirical evaluations, showing that ForM outperforms baseline flow matching methods in generative tasks and validating the effectiveness of its velocity constraint through ablation studies.

These contributions illustrate the promise of force-based methods in generative modeling, emphasizing their capability for stable, efficient, and flexible sampling. This work not only extends our understanding of generative techniques but also lays the foundation for exploring novel high-dimensional generative frameworks that effectively integrate stability and efficiency.

Roadmap. In Section 2, we introduce related work of generative models and flow matching. Then, Section 3 introduces the preliminary of Force Matching. We then propose the Force Matching architecture in Section 4. Section 5 demonstrates empirical experiments of Force Matching, and Section 6 performs ablation study of Force Matching. Finally, we conclude this paper in Section 8.

2 Related work

Generating Models. Generative models have made significant progress over the last decade, enabling diverse applications such as image synthesis, text generation, and data augmentation. One of the foundational models in this area is the Generative Adversarial Network (GAN) introduced by Goodfellow et al. (2014), which consists of a generator and a discriminator that compete in a zero-sum game, thereby leading to the generation of realistic data samples [GPAM⁺14]. GANs have inspired a variety of derivative architectures aimed at improving stability and quality, including Wasserstein GANs (WGAN), which address the instability issues of GANs by employing a different distance metric [ACB17]. Conditional GANs (cGANs) extend the GAN framework to generate data conditioned on additional information, making them more controllable [MO14].

Variational Autoencoders (VAEs), proposed by Kingma and Welling (2013), offer another generative approach that combines variational inference with neural networks to learn a latent variable model of data [KW13]. Unlike GANs, VAEs maximize a lower bound on the log-likelihood of the data, allowing for a more principled probabilistic interpretation. The introduction of the reparameterization trick was key to making VAEs feasible to train with stochastic gradient descent, which has had a considerable impact on the field of deep generative models. Recently, autoregressive models such as PixelCNN [OKK16] and Transformer-based models [VSP⁺17] have demonstrated impressive performance in tasks like image and text generation. These models learn to predict the next element in a sequence, thereby allowing them to generate samples one step at a time, which has proven particularly effective for generating sequential data such as text and audio.

The development of large-scale language models like GPT-3 [BMR⁺20] has further showcased the power of autoregressive architectures in generating coherent and contextually relevant long text, significantly advancing the state-of-the-art in natural language processing. Another line of work explores diffusion models, such as Denoising Diffusion Probabilistic Models (DDPMs), which have gained attention for their ability to generate high-quality images by modeling the process of gradually adding noise to data and then learning to reverse this process [HJA20b]. These models provide an alternative to GANs by optimizing likelihood-based objectives, which makes training more stable. DDPMs have set new benchmarks for image generation quality, rivaling the output of GANs while avoiding some of their training difficulties. These developments collectively showcase the evolution of generative models from adversarial training with GANs to likelihood-based training with VAEs, autoregressive models, e.g. Visual autoregressive modeling (VAR) [TJY⁺24], and diffusion-based approaches, e.g., DDPM [HJA20b]. Each of these methods contributes unique strengths and capabilities, advancing the scope and quality of generated data.

Flow Matching. Flow matching [DLT⁺24, YLP⁺24, GDB⁺24, CGL⁺25] is a key concept in fields such as optimal transport, computer vision, and machine learning, where it has been extensively studied and utilized to align two distributions effectively. The method has roots in the classic work on optimal transport theory, where Monge and Kantorovich initially laid out the foundational ideas for mapping mass distributions with minimal cost [Mon81, Kan42]. Building upon these ideas, Villani expanded the theoretical framework of optimal transport, leading to a rigorous mathematical foundation for flow matching and its related applications [Vil08].

Recent advances in machine learning have leveraged flow matching for deep generative modeling tasks. Denoising diffusion probabilistic models (DDPMs), for example, have drawn inspiration from flow-based methods to improve the stability and efficiency of training [HJA20b]. Similarly, score-based generative models utilize a stochastic differential equation approach to approximate flows, effectively creating a flow-matching procedure for generating realistic data samples [SSDK⁺21]. This approach has demonstrated considerable success in capturing complex, high-dimensional data dis-

tributions. Another relevant development in this domain is the introduction of continuous normalizing flows (CNFs) by Chen et al., which formulated generative modeling as a continuous-time flow process, further refining flow-matching techniques for density estimation and improving scalability [CRBD18]. Grathwohl et al. expanded upon this idea by demonstrating how flow matching could be combined with probability density estimation to achieve more efficient generative models [GCB⁺18]. These works have collectively highlighted the flexibility of flow matching as a tool for a wide range of machine learning tasks, including unsupervised learning, density estimation, and data synthesis. Moreover, applications in computer vision often rely on flow matching to solve challenging problems such as image registration and optical flow estimation. For instance, deep learning-based approaches have integrated flow matching concepts to align images effectively, demonstrating significant improvements over traditional techniques [DFI⁺15, IMS⁺17]. FlowNet and its successor FlowNet2 provide compelling evidence of how flow matching can be operationalized within deep neural architectures to solve real-world vision tasks with state-of-the-art accuracy. Video Latent Flow Matching [CSY25, JSL⁺24, DSF23] incorporates flow matching for temporally coherent video generation. Moreover, numerous recent works [ZCWT23, LSS⁺24a, CLS⁺24, LSS⁺24b, WXZ⁺24, WCZ⁺23, CGL⁺25, XLC⁺24, WCY⁺23, SPH⁺23, CXJ24, FJL⁺24, KLL⁺25a, KLL⁺25b, CLL⁺25b, KLS⁺25, LSS24, CLL⁺25a, LSSZ24, LLSS24, LZW⁺24, HWL⁺24b, HWL⁺24a, SSZ⁺25a, SSZ⁺25b] have significantly inspired and influenced our work.

3 Preliminary

In Section 3.1, we introduce all the notations we used in our paper. Then, in Section 3.2, we show the basic facts about flow matching. In Section 3.3, we present the basic background of special relativity and define the relativistic force.

3.1 Notations

For any positive integer n , we use $[n]$ to denote set $\{1, 2, \dots, n\}$. For two vectors $x \in \mathbb{R}^n$ and $y \in \mathbb{R}^n$, we use $\langle x, y \rangle$ to denote the inner product between x, y . For a vector $v \in \mathbb{R}^n$, we use $\|v\|_2$ to denote the ℓ_2 -norm of v . We use $\mathbf{1}_n$ to denote a length- n vector where all the entries are ones. We use the symbol \perp to represent a component that is perpendicular to the direction of velocity, as exemplified by $a_{\perp t}$, which denotes the perpendicular acceleration. Similarly, the symbol \parallel is employed to indicate a component parallel to the direction of velocity, such as $f_{\parallel t}$, which represents the parallel force. We use \dot{x}_t to denote $\frac{dx_t}{dt}$, and \ddot{x}_t to denote $\frac{d^2x_t}{dt^2}$.

3.2 Flow Matching

Flow Matching (FM) [LCBH⁺22, LGL22] is a generative modeling technique that constructs a smooth, invertible (i.e., diffeomorphic) mapping from a simple prior distribution to a complex target distribution. In FM, a time-dependent mapping Z_t is defined to evolve according to an ordinary differential equation (ODE) driven by a vector field:

$$\frac{dx_t}{dt} = V_t(x_t), \quad t \in [0, T].$$

The goal is to ensure that, at the terminal time T , the ODE transforms a sample x_0 from a simple distribution (e.g., a Gaussian) into a sample x_T from the target data distribution \mathcal{D} .

To achieve this, Flow Matching (FM) constructs a stochastic interpolation between a sample $x_1 \sim \mathcal{D}$ and a sample x_0 drawn from a known prior distribution, typically $\mathcal{N}(0, I)$. The interpolation

is defined as

$$x_t := \alpha_t x_1 + \sigma_t x_0, \quad t \in [0, T],$$

where the time-dependent coefficients α_t and σ_t are chosen so that

$$\alpha_0 = 0, \quad \sigma_0 = 1, \quad \alpha_T = 1, \quad \sigma_T = 0.$$

Thus, at $t = 0$ the interpolated sample is purely the prior (x_0), and at $t = T$ it becomes a data sample (x_1).

The instantaneous change of x is obtained by differentiating the interpolation:

$$\frac{dx_t}{dt} = \frac{d\alpha_t}{dt} x_1 + \frac{d\sigma_t}{dt} x_0.$$

The vector field is approximated by a neural network $V_t(x_t)$ with learnable parameters θ . The FM training objective is then given by

$$\mathcal{L}_{\text{FM}}(\theta) := \mathbb{E}_{t \sim \text{Uniform}[0, T], x_1 \sim \mathcal{D}} [\|V_t(x_t) - v_t(x_t)\|_2^2].$$

This loss ensures that the learned velocity field $V_t(x_t)$ closely tracks the conditional dynamics $v_t(x_t)$ along the interpolation path.

After training, samples are generated by solving the ODE

$$\frac{dx_t}{dt} = V_t(x_t),$$

starting from an initial sample $x_0 \sim \mathcal{N}(0, I)$. Integrating this ODE from $t = 0$ to $t = T$ yields a sample x_T that approximates a draw from the target distribution. This ODE-based formulation offers a flexible and powerful framework for modeling complex data distributions while naturally incorporating conditional sampling.

3.3 Background on Special Relativity

We first introduce several essential ideas of special relativity [E⁺05].

Definition 3.1 (Lorentz Factor). *According to special relativity [E⁺05], the Lorentz factor at lab time t is given by*

$$\gamma_t := \frac{1}{\sqrt{1 - \|v_t^{\text{lab}}\|_2^2/c^2}},$$

where v_t^{lab} is the velocity at lab frame of reference, $c = 3 \times 10^8$ is the speed of light in vacuum.

Then, we introduce the proper time of special relativity.

Definition 3.2 (Proper Time). *The proper time is defined as the time interval measured in the rest frame of a moving object according to special relativity [E⁺05]. The differential form of the proper time is given by*

$$d\tau = \frac{dt}{\gamma_t},$$

where dt is the time interval in the laboratory frame of reference, and γ_t is the Lorentz factor at time lab time t as defined in Definition 3.1.

Next, we define the force under special relativity here.

Definition 3.3 (Relativistic Force). *In the framework of special relativity, the local force (i.e., the force measured in the instantaneous rest frame of the particle) denoted as f^{local} has*

$$f^{\text{local}} := \frac{dp^{\text{lab}}}{d\tau}, \quad (1)$$

where p^{lab} is the momentum at lab frame of reference, τ denotes the proper time defined in Definition 3.2.

The momentum in the lab frame is defined as

$$p^{\text{lab}} := m^{\text{lab}}v_t^{\text{lab}}, \quad (2)$$

where m^{lab} is the mass at lab frame of reference, and v_t^{lab} is the velocity at lab frame of reference.

We state an equivalence lemma. Due to the space limitation, we delayed the proofs into the appendix.

Lemma 3.4 (Equivalent Form of Relativistic Force, informal version of Lemma A.5). *Let p^{lab} be the momentum defined in Eq. (2), γ_t be the Lorentz factor at lab time t defined in Definition 3.1, τ denotes the proper time, $v_t^{\text{lab}} = \dot{x}_t$ denotes the velocity, $a_t^{\text{lab}} = \ddot{x}_t$ denotes the acceleration. The relativistic force, defined as the time derivative of the momentum in the lab frame, can be written as*

$$f^{\text{local}} = m^{\text{lab}}(\gamma_t a_t^{\text{lab}} + \gamma_t^3 \frac{\langle v_t^{\text{lab}}, a_t^{\text{lab}} \rangle}{c^2} v_t^{\text{lab}}).$$

4 Force Matching

In this section, we introduce Force Matching (ForM), a new architecture for generative models, and provide its theoretical analysis. In Section 4.1, we introduce the training objective of Force Matching. Then, in Section 4.2. In Section 4.3, we illustrate and discuss the speed limitation of ForM. In Section 4.4, We show the interpolation path for ForM.

4.1 Definition of Force Matching Objective

Next, we define the training objective of Force Matching.

Definition 4.1 (Force Matching Objective). *The training objective of Force Matching (ForM) is defined by*

$$\mathcal{L}_{\text{ForM}}(\theta) := \mathbb{E}_{t \sim \text{Uniform}[0, T], x_1 \sim \mathcal{D}} [\|F_t(x_t) - f_t(x_t)\|_2^2],$$

where \mathcal{D} is the target data distribution, $f_t(x_t)$ is the target relativistic force defined in Definition 3.3, and $F_t(x)$ is a trainable neural network parameterized with θ .

4.2 Our Result I: Sampling ODE

We define an ordinary differential equation (ODE) in order to get the position based on a given relativistic force.

Theorem 4.2 (Sampling ODE, informal version of Theorem A.1). *Giving the force at position x_t denoted as $f_t(x_t)$, we could solve for ForM sampling path x_t by the following ODE*

$$\ddot{x}_t = \frac{1}{m^{\text{lab}}\gamma_t} \left(f_t^{\text{local}} - \frac{\langle v_t^{\text{lab}}, f_t^{\text{local}} \rangle}{c^2} v_t^{\text{lab}} \right),$$

where $x_0 \sim \mathcal{N}(0, I)$, $\dot{x}_0 = 0$.

Theorem 4.2 shows how to derive the position x_t from the relativistic force field $f_t(x_t)$. Unlike first-order flow-based methods, ForM naturally involves a second-order ODE because it encodes the evolution of both position and velocity under relativistic constraints. This allows for more expressive and physically-motivated sampling trajectories, where velocity constraints can help stabilize the generative process. Once a neural network $F_t(x)$ is trained to approximate $f_t(x)$, the sampling procedure integrates this second-order ODE to produce samples consistent with the target distribution.

4.3 Our Result II: Speed Limit

One property of relativistic mechanics is the velocity will always be under the constant c , which is the speed of light.

In reality, the speed of light is $c \approx 3 \times 10^8$. For any v_t , the speed $\|v_t\|_2$ can approach but never exceed c . This property stabilizes the generating process. We formalize and prove this in Theorem 4.3.

Theorem 4.3 (Speed Limit, informal version of Theorem A.3). *For a ForM model with sampling path $x : [0, T] \rightarrow \mathbb{R}^n$, the velocity satisfies*

$$\|\dot{x}_t\|_2 < c \quad , \forall t \in [0, T].$$

It shows that the sample velocity remains strictly below c at all times under relativistic constraints. Practically, this upper bound on velocity helps mitigate risks of numerical instability or “exploding gradients” that can sometimes arise in diffusion- or flow-based generative models. By capping the speed of samples, ForM maintains a controlled and stable evolution in high-dimensional spaces. This provides a theoretical guarantee of safety against runaway behaviors, making the sampling process more robust.

4.4 Our Result III: ForM with TrigFlow

The interpolation path of ForM is given by the following theorem.

Theorem 4.4 (ForM with TrigFlow, informal version of Theorem A.4). *We let $m = 1$ for simplicity in ForM. Giving a the interpolation $x_t = \alpha_t x_1 + \sigma_t x_0$, where $\alpha_T = 1$, $\alpha_0 = 0$, $\sigma_T = 0$, $\sigma_0 = 1$. We let $F_t(x_t)$ denote a vector map of force, a trainable neuron network parameterized with θ . We select the α_t and σ_t identical with TrigFlow [LS24], where $\alpha_t = \sin(t)$ and $\sigma_t = \cos(t)$, $T = \frac{\pi}{2}$. Then, force interpolation could be simplified to*

$$f_t(x_t) = \frac{(\cos(t)x_1 - \sin(t)x_0) \cdot (-\sin(t)x_1 - \cos(t)x_0)}{c^2 - (\cos(t)x_1 - \sin(t)x_0)^2} (\cos(t)x_1 - \sin(t)x_0).$$

Theorem 4.4 highlights how the ForM framework can be directly coupled with trigonometric interpolation paths. By choosing α_t and σ_t as sine and cosine, respectively, we obtain a closed-form expression for the relativistic force that governs the sample evolution. This synergy suggests that ForM can not only unify different flow-based or diffusion-based models but also inherit the continuous-time advantages of the TrigFlow parameterization. Consequently, one can design more flexible interpolation strategies while still enjoying the stability benefits of relativistic velocity constraints.

5 Experiment

Algorithm 1 First-order Training, [LGL22]

```

1: procedure 1STTRAINING( $\theta, D$ )
2:                                     ▷ Parameter  $\theta$  for the model  $u_1$ 
3:                                     ▷ Training dataset  $D$ 
4:   while not converged do
5:     /* Sample a trajectory from dataset. */
6:     /*  $x_t$  denotes the position at time  $t$ . */
7:     /*  $\dot{x}_t$  denotes the velocity at time  $t$ . */
8:      $\{x_t\}_{t \in [0,1]}, \{\dot{x}_t\}_{t \in [0,1]} \sim D$ 
9:     /* Random sample a timestep  $t$ . */
10:     $t \sim \mathcal{U}(0, 1)$ 
11:    /* Update model parameter  $\theta$ . */
12:     $\theta \leftarrow \nabla_{\theta}(\|u_1(x_t, t) - \dot{x}_t\|_2^2)$ 
13:  end while
14:  return  $\theta$ 
15: end procedure

```

Algorithm 2 First-order Sampling, [LGL22]

```

1: procedure 1STDSAMPLING( $\theta, M$ )
2:                                     ▷ Parameter  $\theta$  for the model  $u_1$ 
3:                                     ▷ The number of sampling steps  $M$ 
4:    $x \sim \mathcal{N}(0, I)$ 
5:    $d \leftarrow 1/M$ 
6:    $t \leftarrow 0$ 
7:   for  $n \in [0, \dots, M - 1]$  do
8:      $x \leftarrow x + d \cdot u_1(x, t)$ 
9:      $t \leftarrow t + d$ 
10:  end for
11:  return  $x$ 
12: end procedure

```

In this section, we conduct a systematic evaluation of Force Matching (ForM) effectiveness through extensive experimentation, emphasizing its significant role in advancing distribution generation. Section 5.1 describes the experimental framework, encompassing the Onedot, Halfmoons, and Spiral datasets, force dynamics, and a comparative analysis of various trajectory evolution

Algorithm 3 First and Second-order Training

```
1: procedure 2NDTRAINING( $\theta, D$ )
2:                                      $\triangleright$  Parameter  $\theta$  for the models  $u_1$  and  $u_2$ 
3:                                      $\triangleright$  Training dataset  $D$ 
4:   while not converged do
5:     /* Random sample a trajectory from dataset. */
6:     /*  $x_t$  denotes the position at time  $t$ . */
7:     /*  $\dot{x}_t$  denotes the velocity at time  $t$ . */
8:     /*  $\ddot{x}_t$  denotes the acceleration at time  $t$ . */
9:      $\{x_t\}_{t \in [0,1]}, \{\dot{x}_t\}_{t \in [0,1]}, \{\ddot{x}_t\}_{t \in [0,1]} \sim D$ 
10:    /* Random sample a timestep  $t$ . */
11:     $t \sim \mathcal{U}(0, 1)$ 
12:    /* Update model parameter  $\theta$ . */
13:     $\theta \leftarrow \nabla_{\theta} (\|u_1(x_t, t) - \dot{x}_t\|_2^2$ 
         $+ \|u_2(u_1(x_t, t), x_t, t) - \ddot{x}_t\|_2^2)$ 
14:  end while
15:  return  $\theta$ 
16: end procedure
```

Algorithm 4 First and Second-order Sampling

```
1: procedure 2NDSAMPLING( $\theta, M$ )
2:                                      $\triangleright$  Parameter  $\theta$  for the models  $u_1$  and  $u_2$ 
3:                                      $\triangleright$  The number of sampling steps  $M$ 
4:    $x \sim \mathcal{N}(0, I)$ 
5:    $d \leftarrow 1/M$ 
6:    $t \leftarrow 0$ 
7:   for  $n \in [0, \dots, M - 1]$  do
8:      $x \leftarrow x + d \cdot u_1(x, t) + \frac{d^2}{2} \cdot u_2(u_1(x, t), x, t)$ 
9:      $t \leftarrow t + d$ 
10:  end for
11:  return  $x$ 
12: end procedure
```

methods. Section 5.2 examines qualitative outcomes, demonstrating how second-order terms refine trajectory smoothness and highlighting ForM’s superiority in transport dynamics modeling.

5.1 Experiment setup

For an in-depth trajectory evolution analysis, we assess three approaches: the standard flow matching [LCBH⁺22] method utilizing only the first-order term, an improved approach integrating both first-order and second-order terms, and our proposed ForM model on three kinds of complex and challenging datasets.

Datasets. (1) Onedot dataset: As illustrated in Figure 1, the Onedot dataset comprises 200 points sampled from a Gaussian distribution with variance 0.3 to establish the central source distribution. The target distribution is generated via a Lorentz field, where each point’s initial velocity matches

Algorithm 5 ForM Training, (Ours)

```
1: procedure FORMTRAINING( $\theta, D, p, k$ )
2:                                      $\triangleright$  Parameter  $\theta$  for the ForM model  $F_\theta$ 
3:                                      $\triangleright$  Training dataset  $D$ 
4:                                      $\triangleright$  Stepsize and time index distribution  $p$ 
5:                                      $\triangleright$  Batch size  $k$ 
6:   while not converged do
7:     /* Random sample a trajectory from dataset. */
8:     /*  $x_t$  denotes the position at time  $t$ . */
9:     /*  $f_t$  denotes the Lorentz force at time  $t$ . */
10:     $\{x_t\}_{t \in [0,1]}, \{f_t\}_{t \in [0,1]} \sim D$ 
11:    /* Random sample a timestep  $t$ . */
12:     $t \sim \mathcal{U}(0, 1)$ 
13:    /* Update model parameter  $\theta$ . */
14:     $\theta \leftarrow \nabla_\theta(\|F_\theta(t) - f_t\|_2^2)$ 
15:  end while
16:  return  $\theta$ 
17: end procedure
```

Algorithm 6 ForM Sampling, (Ours)

```
1: procedure FORMSAMPLING( $\theta, M$ )
2:                                      $\triangleright$  Parameter  $\theta$  for the ForM model  $F_\theta$ 
3:                                      $\triangleright$  The number of sampling steps  $M$ 
4:    $x \sim \mathcal{N}(0, I)$ 
5:    $d \leftarrow 1/M$ 
6:    $t \leftarrow 0$ 
7:   for  $n \in [0, \dots, M - 1]$  do
8:     /* Get Lorentz force  $f_L$  via model  $F_\theta$ . */
9:      $f_L \leftarrow F_\theta(t)$ 
10:    /* Calculate acceleration  $a$  via Theorem 4.2. */
11:     $a \leftarrow \phi(v_{\text{prev}}, f_L)$ 
12:    /* Calculate velocity  $v$ . */
13:     $v \leftarrow v_{\text{prev}} + d a_t$ 
14:    /* Calculate  $x$ . */
15:     $x \leftarrow x_{\text{prev}} + d (v_t + v_{\text{prev}})/2$ 
16:    /* Update  $t$ . */
17:     $t \leftarrow t + d$ 
18:    /* Store variables for next iteration. */
19:     $x_{\text{prev}} \leftarrow x$ 
20:     $v_{\text{prev}} \leftarrow v$ 
21:  end for
22:  return  $x$ 
23: end procedure
```

its initial position vector. The parallel force is defined as $\gamma^3 m_0 a_x$, while the perpendicular force follows $\gamma m_0 a_x$, where $\gamma = (1 - v^2/c^2)^{-\frac{1}{2}}$, and the speed of light is set to $c = 3 \times 10^8$ m/s. In the

Algorithm 7 Numerical ODE Solver

```
1: procedure NUMERICALODESOLVER( $\theta, M$ )
2:                                      $\triangleright$  Parameter  $\theta$  for the ForM model  $F_t$ 
3:                                      $\triangleright$  The number of sampling steps  $M$ 
4:    $x \sim \mathcal{N}(0, I)$ 
5:    $d \leftarrow 1/M$ 
6:    $t \leftarrow 0$ 
7:   for  $n \in [0, \dots, M - 1]$  do
8:     /* Solve the ODE in Theorem 4.2. */
9:      $x \leftarrow \text{ODESolver}(x, \frac{dx}{dt}, F(t), d)$ 
10:     $t \leftarrow t + d$ 
11:   end for
12:   return  $x$ 
13: end procedure
```

Onedot dataset, both forces are set to 1.5×10^8 , with a duration of 1s.

(2) Halfmoons dataset: Then, as illustrated in Figure 2, we sampled 1000 dots from a central source distribution, and the target distribution is generated by a Lorentz field. For the dots above the x -axis, we set the direction of their velocity parallel to the x -axis to the right, and the dots below the x -axis are parallel to the x -axis to the left. And the parallel force denoted as $1 \times 10^7 \cdot \sin(t)$, the perpendicular force follows $7 \times 10^8 \cdot \sin(8t)$.

(3) Spiral dataset: With reference to the Spiral dataset as shown in Figure 3, 1000 data points were extracted from a central source distribution, and the target distribution was similarly synthesized via a Lorentz field. In this instance, the source distribution was segmented into two components—a circular core and an annular ring—by equally partitioning the original radius. The initial velocity assigned to each point was determined by both its designated segment and the angular coordinate of its starting position. As a result, points residing in the ring attain comparatively greater initial speeds, and those with larger angular coordinates likewise manifest enhanced velocities. Finally, the parallel force is specified by $1 \times 10^7 \cdot \sin(t)$, while the perpendicular force is given by $7 \times 10^8 \cdot \sin(t)$.

Baselines. We compare our ForM model with two traditional yet powerful baselines. The first baseline is standard flow matching, which models the transfer trajectory between distributions using the first-order velocity of the trajectory. We denote this method as O1 (Algorithm 1 and 2). The second baseline is an improved version of the first-order approach, incorporating both first-order velocity and second-order acceleration to model the trajectory, which we denote as O1+O2 (Algorithm 3 and 4). Both baselines rely on modeling the higher-order derivatives of the trajectory. In contrast, our ForM model (Algorithm 5 and 6) introduces a novel approach by modeling the Lorentz force acting on the trajectory within a field, offering a fundamentally different perspective on learning the target distribution. This represents a new modeling paradigm that extends beyond conventional flow-based methods.

5.2 Results analysis

This section presents a comparative analysis of trajectory evolution on the *Onedot* and *Halfmoons* datasets. Figure 4 illustrates the trajectories generated by three approaches: (i) the original flow matching method that utilizes only the first-order term (denote as O1), (ii) an enhanced variant

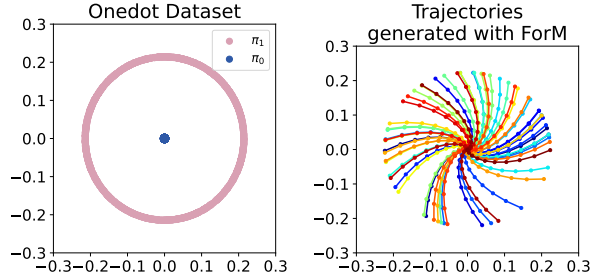


Figure 1: Left: Onedot Dataset. The objective is to train the ForM model to learn a transport trajectory from distribution π_0 (**blue**) to distribution π_1 (**pink**). Right: The transportation trajectory generated by the ForM model.

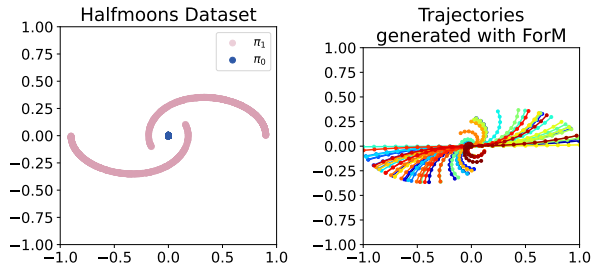


Figure 2: Left: Halfmoons Dataset. The objective is to train ForM to learn a transport trajectory from distribution π_0 (**blue**) to distribution π_1 (**pink**). Right: The transportation trajectory generated by the ForM model.

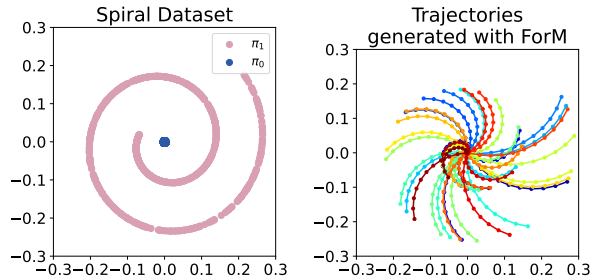


Figure 3: Left: Spiral Dataset. The objective is to train the ForM model to learn a transport trajectory from distribution π_0 (**blue**) to distribution π_1 (**pink**). Right: The transportation trajectory generated by the ForM model.

that incorporates both first- and second-order terms (denote as O1+O2), and (iii) our proposed Force Matching model (denote as ForM) which explicitly integrates the influence of a Lorentz force field.

Although the inclusion of the second-order term introduces additional dynamic information, the enhanced variant still fails to capture the complex transportation trajectories required by these datasets. In contrast, by modeling the potential Lorentz force, the ForM model markedly improves performance. This integration acts as a guiding mechanism, effectively steering the model toward a more accurate approximation of the target distribution. In other words, the physics-inspired addition of the Lorentz force facilitates the learning process, enabling the model to navigate the intricacies of the complex transport dynamics more efficiently.

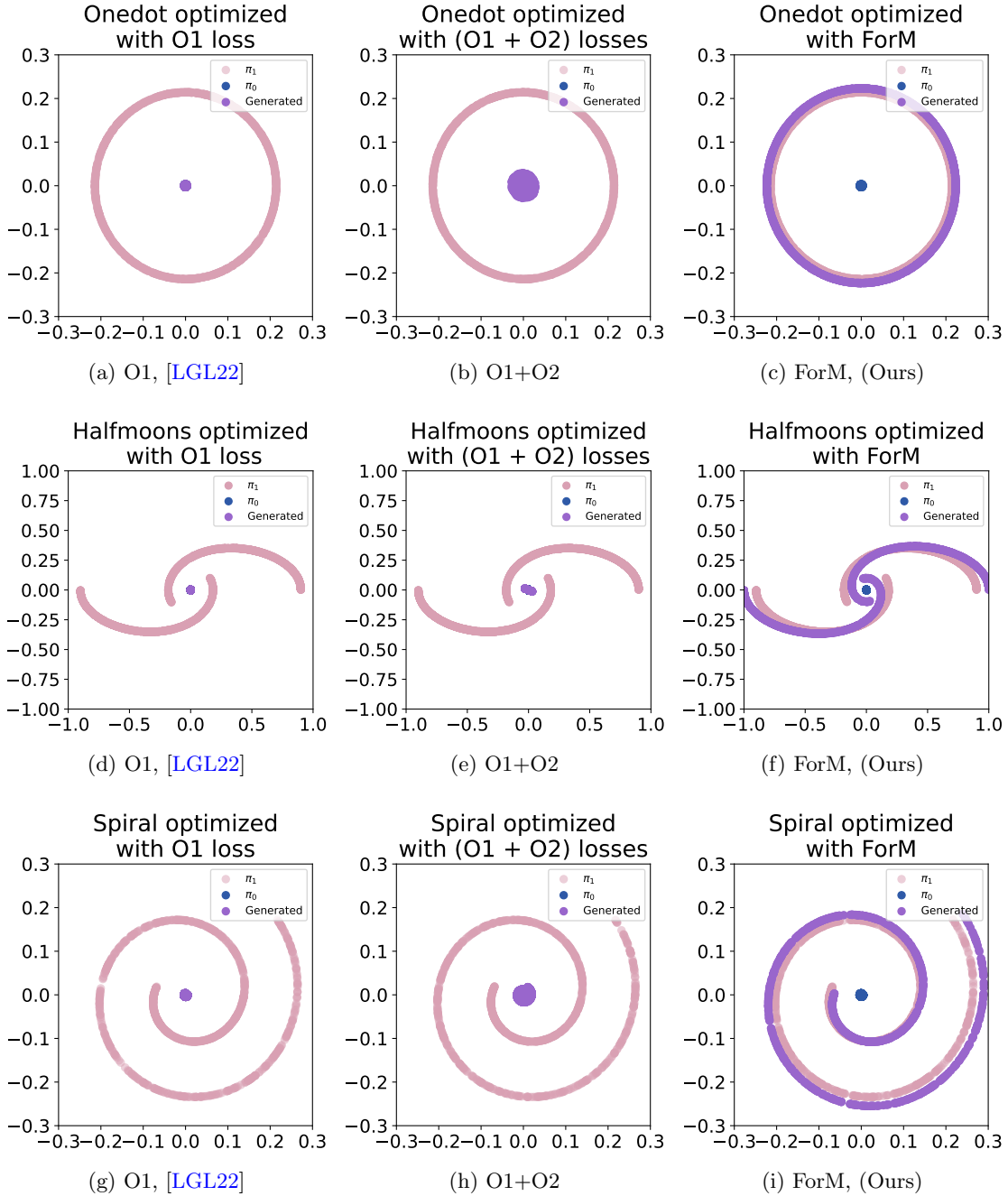


Figure 4: **Left:** Flow matching [LCBH⁺22] using only the first-order term. **Middle:** An improved method that incorporates both first- and second-order terms. **Right:** Our proposed ForM model applied to the Onedot, Halfmoons, and Spiral datasets. Note that the first-order method (O1) fails to capture the target distribution, and although the second-order method (O2) exhibits slight improvement, it still does not adequately model the target distribution. In contrast, by leveraging the Lorentz force to guide the trajectory evolution, the ForM model significantly enhances the accuracy of the target distribution, as further evidenced by the quantitative results in Table 1.

This qualitative improvement is further substantiated by the quantitative results reported in Table 1, where the ForM model achieves the lowest Euclidean distance loss among the three methods. These findings confirm that incorporating domain-specific forces, such as the Lorentz force, can significantly enhance the modeling of complex transport phenomena.

5.3 Euclidean distance loss

This section quantitatively assesses different approaches using Euclidean distance loss, which quantifies the deviation between transported and target distributions. Table 1 presents the loss values across three methods on the Onedot dataset and Halfmoons dataset, the unit we use is 0.1 light seconds. Lower values indicate higher precision in distribution transfer. The results demonstrate that incorporating the second-order term (O1 + O2) enhances performance beyond the first-order term (O1) alone. Notably, ForM surpasses both baselines, achieving the lowest Euclidean distance loss, reinforcing its effectiveness in modeling transport trajectories.

Table 1: **Euclidean distance loss across three methods: Flow matching [LCBH⁺22] with the first order term (O1), an advanced version integrating both first order and second order terms (O1 + O2), and our proposed ForM on the Onedot dataset and Halfmoons dataset.** Lower values represent greater accuracy in distribution transfer. The optimal values are displayed in **bold**, while the second-best values are underlined. The qualitative results are provided in Figure 4.

Loss terms	Onedot	Halfmoons	Spiral
O1, [LGL22]	2.146	5.853	1.666
O1 + O2	<u>2.048</u>	<u>5.793</u>	<u>1.578</u>
ForM, (Ours)	0.509	0.714	0.124

6 Empirical Ablation Study

In this section, we empirically evaluate the performance of our proposed ForM model through a series of ablation experiments. We begin by illustrating the Spiral dataset and the corresponding transport objective, where samples are moved from the distribution π_0 (**blue**) to π_1 (**pink**) (see Figure 3). We then compare three approaches: the baseline Flow matching method using solely the first-order term (O1), an enhanced variant that integrates both first-order and second-order loss metrics (O1 + O2), and our ForM model that leverages the Lorentz force to guide trajectory evolution. Qualitative results are shown in Figure 4, while Table 1 quantitatively demonstrates the superior performance of the ForM model.

7 Discussion

The core motivation behind the Force Matching (ForM) model stems from the need to stabilize generative modeling processes, particularly in flow-based methods where uncontrolled velocity magnitudes can lead to instability during sampling. Traditional approaches, such as Flow Matching (FM), offer different perspectives on modeling data evolution, yet they often lack explicit constraints that regulate sample movement, which can hinder both stability and efficiency. Inspired by special relativistic mechanics, we introduce a principled way to control velocity magnitudes through

the Lorentz factor, ensuring that sample velocities remain bounded during the generative process. This formulation draws a parallel between relativistic motion and generative trajectories, where limiting sample speed prevents erratic behaviors and enhances robustness. By enforcing this constraint, ForM provides a novel perspective on generative modeling that aligns with both theoretical principles and practical stability considerations.

While ForM establishes a strong foundation for stable generative modeling, several exciting directions remain open for further exploration. Extending ForM to high-dimensional image and video generation tasks would be a crucial next step, requiring efficient implementations of relativistic constraints in large-scale neural networks. Additionally, investigating how ForM’s velocity constraint can be integrated into score-based generative models could lead to hybrid approaches that combine the strengths of both paradigms. Another promising direction is the development of adaptive or learnable velocity constraints that dynamically regulate sample movement based on data complexity, potentially enhancing flexibility. More broadly, the incorporation of relativistic principles into generative modeling raises questions about the role of physics-inspired constraints in deep learning. Finally, the implicit connection between ForM and optimal transport theory suggests that deeper theoretical investigations in this direction could lead to new generative frameworks grounded in optimal transport principles. By leveraging insights from physics and generative modeling, ForM paves the way for designing more stable, efficient, and interpretable generative models, inspiring further research into force-based approaches and their applications to complex data synthesis tasks.

8 Conclusion

In this work, we introduce Force Matching (ForM), an innovative and comprehensive framework for generative modeling. ForM incorporates the principles of relativistic mechanics, higher-order flow matching, and TrigFlow, forming a unique and powerful synergy. The core idea behind ForM is to model the generative process in a way that accounts for both the geometric and dynamic aspects of flow, inspired by relativistic mechanics. We demonstrate that ForM not only preserves the structure of the data but also introduces an additional layer of stability to the generative process. Specifically, we theoretically prove that ForM bounds the velocity of the generative process under a hyperparameter c during the sampling procedure, which leads to improved control and stabilization of the process. This stabilization mechanism mitigates issues such as mode collapse and sampling instability that often plague other generative models. Through extensive empirical experiments, we demonstrate that ForM outperforms both Flow Matching and second-order Flow Matching in terms of generative quality and sample diversity. These results highlight the effectiveness of incorporating higher-order dynamics and relativistic principles into the generative process. Additionally, we conduct an ablation study to evaluate the individual components of ForM, further demonstrating its superiority over existing methods. This analysis confirms the contribution of each aspect of the framework, such as the higher-order flow matching and relativistic dynamics, to its overall performance. ForM offers a fresh perspective on the understanding of Flow Matching within the context of relativistic mechanics, presenting a new paradigm in the field of generative modeling. By redefining the conceptual and practical foundations of generative processes, ForM sets a new benchmark for the future development of generative models.

References

- [ACB17] Martin Arjovsky, Soumith Chintala, and Léon Bottou. Wasserstein gan. *arXiv preprint arXiv:1701.07875*, 2017.
- [BMR⁺20] Tom B Brown, Benjamin Mann, Nick Ryder, Melanie Subbiah, Jared Kaplan, Prafulla Dhariwal, Arvind Neelakantan, Pranav Shyam, Girish Sastry, Amanda Askell, et al. Language models are few-shot learners. *Advances in neural information processing systems*, 33:1877–1901, 2020.
- [CGL⁺25] Yuefan Cao, Chengyue Gong, Xiaoyu Li, Yingyu Liang, Zhizhou Sha, Zhenmei Shi, and Zhao Song. Richspace: Enriching text-to-video prompt space via text embedding interpolation. *arXiv preprint arXiv:2501.09982*, 2025.
- [CLL⁺25a] Yuefan Cao, Xiaoyu Li, Yingyu Liang, Zhizhou Sha, Zhenmei Shi, Zhao Song, and Jiahao Zhang. Dissecting submission limit in desk-rejections: A mathematical analysis of fairness in ai conference policies. *arXiv preprint arXiv:2502.00690*, 2025.
- [CLL⁺25b] Yifang Chen, Xiaoyu Li, Yingyu Liang, Zhenmei Shi, and Zhao Song. Universal approximation of visual autoregressive transformers. *arXiv preprint arXiv:2502.06167*, 2025.
- [CLS⁺24] Bo Chen, Yingyu Liang, Zhizhou Sha, Zhenmei Shi, and Zhao Song. Hsr-enhanced sparse attention acceleration. *arXiv preprint arXiv:2410.10165*, 2024.
- [CRBD18] Tian Qi Chen, Yulia Rubanova, Jesse Bettencourt, and David Duvenaud. Neural ordinary differential equations. In *Advances in Neural Information Processing Systems (NeurIPS)*, 2018.
- [CSY25] Yang Cao, Zhao Song, and Chiwun Yang. Video latent flow matching: Optimal polynomial projections for video interpolation and extrapolation. *arXiv preprint arXiv:2502.00500*, 2025.
- [CXJ24] Zirui Cheng, Jingfei Xu, and Haojian Jin. Treequestion: Assessing conceptual learning outcomes with llm-generated multiple-choice questions. *Proceedings of the ACM on Human-Computer Interaction*, 8(CSCW2):1–29, 2024.
- [DFI⁺15] Alexey Dosovitskiy, Philipp Fischer, Eddy Ilg, Philip Hausser, Caner Hazirbas, Vladimir Golkov, Patrick van der Smagt, Daniel Cremers, and Thomas Brox. FlowNet: Learning optical flow with convolutional networks. In *IEEE International Conference on Computer Vision (ICCV)*, 2015.
- [DLT⁺24] Wei Deng, Weijian Luo, Yixin Tan, Marin Biloš, Yu Chen, Yuriy Nevmyvaka, and Ricky TQ Chen. Variational schrödinger diffusion models. *arXiv preprint arXiv:2405.04795*, 2024.
- [DN21] Prafulla Dhariwal and Alexander Nichol. Diffusion models beat gans on image synthesis. *Advances in neural information processing systems*, 34:8780–8794, 2021.
- [DSF23] Aram Davtyan, Sepehr Sameni, and Paolo Favaro. Efficient video prediction via sparsely conditioned flow matching. In *Proceedings of the IEEE/CVF International Conference on Computer Vision*, pages 23263–23274, 2023.

- [E⁺05] Albert Einstein et al. Zur elektrodynamik bewegter körper. *Annalen der physik*, 17(10):891–921, 1905.
- [EKB⁺24] Patrick Esser, Sumith Kulal, Andreas Blattmann, Rahim Entezari, Jonas Müller, Harry Saini, Yam Levi, Dominik Lorenz, Axel Sauer, Frederic Boesel, et al. Scaling rectified flow transformers for high-resolution image synthesis. In *Forty-first International Conference on Machine Learning*, 2024.
- [FJL⁺24] Tao Feng, Chuanyang Jin, Jingyu Liu, Kunlun Zhu, Haoqin Tu, Zirui Cheng, Guanyu Lin, and Jiaxuan You. How far are we from agi. *arXiv preprint arXiv:2405.10313*, 2024.
- [GCB⁺18] Will Grathwohl, Ricky T. Q. Chen, Jesse Bettencourt, Ilya Sutskever, and David Duvenaud. FFJORD: Free-form continuous dynamics for scalable reversible generative models. In *International Conference on Learning Representations (ICLR)*, 2018.
- [GDB⁺24] Chengyue Gong, Xiaocong Du, Bhargav Bhushanam, Lemeng Wu, Xingchao Liu, Dhruv Choudhary, Arun Kejariwal, and Qiang Liu. Layer compression of deep networks with straight flows. In *Proceedings of the AAAI Conference on Artificial Intelligence*, pages 12181–12189, 2024.
- [GPAM⁺14] Ian Goodfellow, Jean Pouget-Abadie, Mehdi Mirza, Bing Xu, David Warde-Farley, Sherjil Ozair, Aaron Courville, and Yoshua Bengio. Generative adversarial nets. In *Advances in neural information processing systems*, pages 2672–2680, 2014.
- [HJA20a] Jonathan Ho, Ajay Jain, and Pieter Abbeel. Denoising diffusion probabilistic models. *Advances in neural information processing systems*, 33:6840–6851, 2020.
- [HJA20b] Jonathan Ho, Ajay Jain, and Pieter Abbeel. Denoising diffusion probabilistic models. In *Advances in Neural Information Processing Systems*, volume 33, pages 6840–6851, 2020.
- [HWL⁺24a] Jerry Yao-Chieh Hu, Weimin Wu, Yi-Chen Lee, Yu-Chao Huang, Minshuo Chen, and Han Liu. On statistical rates of conditional diffusion transformers: Approximation, estimation and minimax optimality. *arXiv preprint arXiv:2411.17522*, 2024.
- [HWL⁺24b] Jerry Yao-Chieh Hu, Weimin Wu, Zhuoru Li, Sophia Pi, , Zhao Song, and Han Liu. On statistical rates and provably efficient criteria of latent diffusion transformers (dits). *Advances in Neural Information Processing Systems*, 38, 2024.
- [IMS⁺17] Eddy Ilg, Nikolaus Mayer, Tonmoy Saikia, Margret Keuper, Alexey Dosovitskiy, and Thomas Brox. FlowNet2: Evolution of optical flow estimation with deep networks. In *IEEE Conference on Computer Vision and Pattern Recognition (CVPR)*, 2017.
- [JSL⁺24] Yang Jin, Zhicheng Sun, Ningyuan Li, Kun Xu, Hao Jiang, Nan Zhuang, Quzhe Huang, Yang Song, Yadong Mu, and Zhouchen Lin. Pyramidal flow matching for efficient video generative modeling. *arXiv preprint arXiv:2410.05954*, 2024.
- [KAAL22] Tero Karras, Miika Aittala, Timo Aila, and Samuli Laine. Elucidating the design space of diffusion-based generative models. *Advances in neural information processing systems*, 35:26565–26577, 2022.

- [KAL⁺24] Tero Karras, Miika Aittala, Jaakko Lehtinen, Janne Hellsten, Timo Aila, and Samuli Laine. Analyzing and improving the training dynamics of diffusion models. In *Proceedings of the IEEE/CVF Conference on Computer Vision and Pattern Recognition*, pages 24174–24184, 2024.
- [Kan42] Leonid Kantorovich. On the translocation of masses. *Dokl. Akad. Nauk. USSR*, 37:199–201, 1942.
- [KLL⁺25a] Yekun Ke, Xiaoyu Li, Yingyu Liang, Zhizhou Sha, Zhenmei Shi, and Zhao Song. On computational limits and provably efficient criteria of visual autoregressive models: A fine-grained complexity analysis. *arXiv preprint arXiv:2501.04377*, 2025.
- [KLL⁺25b] Yekun Ke, Xiaoyu Li, Yingyu Liang, Zhenmei Shi, and Zhao Song. Circuit complexity bounds for visual autoregressive model. *arXiv preprint arXiv:2501.04299*, 2025.
- [KLS⁺25] Yekun Ke, Yingyu Liang, Zhizhou Sha, Zhenmei Shi, and Zhao Song. Dpbloomfilter: Securing bloom filters with differential privacy. *arXiv preprint arXiv:2502.00693*, 2025.
- [KW13] Diederik P Kingma and Max Welling. Auto-encoding variational bayes. *arXiv preprint arXiv:1312.6114*, 2013.
- [LCBH⁺22] Yaron Lipman, Ricky TQ Chen, Heli Ben-Hamu, Maximilian Nickel, and Matt Le. Flow matching for generative modeling. *arXiv preprint arXiv:2210.02747*, 2022.
- [LGL22] Xingchao Liu, Chengyue Gong, and Qiang Liu. Flow straight and fast: Learning to generate and transfer data with rectified flow. *arXiv preprint arXiv:2209.03003*, 2022.
- [LLSS24] Chenyang Li, Yingyu Liang, Zhenmei Shi, and Zhao Song. Exploring the frontiers of softmax: Provable optimization, applications in diffusion model, and beyond. *arXiv preprint arXiv:2405.03251*, 2024.
- [LS24] Cheng Lu and Yang Song. Simplifying, stabilizing and scaling continuous-time consistency models. *arXiv preprint arXiv:2410.11081*, 2024.
- [LSS⁺24a] Yingyu Liang, Zhizhou Sha, Zhenmei Shi, Zhao Song, and Yufa Zhou. Looped relu mlps may be all you need as practical programmable computers. *arXiv preprint arXiv:2410.09375*, 2024.
- [LSS⁺24b] Yingyu Liang, Zhizhou Sha, Zhenmei Shi, Zhao Song, and Yufa Zhou. Multi-layer transformers gradient can be approximated in almost linear time. *arXiv preprint arXiv:2408.13233*, 2024.
- [LSSS24] Yingyu Liang, Zhizhou Sha, Zhenmei Shi, and Zhao Song. Differential privacy mechanisms in neural tangent kernel regression. *arXiv preprint arXiv:2407.13621*, 2024.
- [LSSZ24] Yingyu Liang, Zhenmei Shi, Zhao Song, and Yufa Zhou. Unraveling the smoothness properties of diffusion models: A gaussian mixture perspective. *arXiv preprint arXiv:2405.16418*, 2024.
- [LZW⁺24] Chengyi Liu, Jiahao Zhang, Shijie Wang, Wenqi Fan, and Qing Li. Score-based generative diffusion models for social recommendations. *arXiv preprint arXiv:2412.15579*, 2024.

- [MO14] Mehdi Mirza and Simon Osindero. Conditional generative adversarial nets. In *arXiv preprint arXiv:1411.1784*, 2014.
- [Mon81] Gaspard Monge. *Memoire sur la theorie des deblais et des remblais*. 1781.
- [OKK16] Aaron van den Oord, Nal Kalchbrenner, and Koray Kavukcuoglu. Pixel recurrent neural networks. In *International conference on machine learning*, pages 1747–1756, 2016.
- [RBL⁺22] Robin Rombach, Andreas Blattmann, Dominik Lorenz, Patrick Esser, and Björn Ommer. High-resolution image synthesis with latent diffusion models. In *Proceedings of the IEEE/CVF conference on computer vision and pattern recognition*, pages 10684–10695, 2022.
- [SDWMG15] Jascha Sohl-Dickstein, Eric Weiss, Niru Maheswaranathan, and Surya Ganguli. Deep unsupervised learning using nonequilibrium thermodynamics. In *International conference on machine learning*, pages 2256–2265. PMLR, 2015.
- [SPH⁺23] Vignesh Ram Somnath, Matteo Pariset, Ya-Ping Hsieh, Maria Rodriguez Martinez, Andreas Krause, and Charlotte Bunne. Aligned diffusion schrödinger bridges. In *Uncertainty in Artificial Intelligence*, pages 1985–1995. PMLR, 2023.
- [SSDK⁺21] Yang Song, Jascha Sohl-Dickstein, Diederik P Kingma, Abhishek Kumar, Stefano Ermon, and Ben Poole. Score-based generative modeling through stochastic differential equations. In *International Conference on Learning Representations (ICLR)*, 2021.
- [SSZ⁺25a] Xuan Shen, Zhao Song, Yufa Zhou, Bo Chen, Yanyu Li, Yifan Gong, Kai Zhang, Hao Tan, Jason Kuen, Henghui Ding, Zhihao Shu, Wei Niu, Pu Zhao, Yanzhi Wang, and Jiuxiang Gu. Lazydit: Lazy learning for the acceleration of diffusion transformers. In *Proceedings of the AAAI Conference on Artificial Intelligence*, 2025.
- [SSZ⁺25b] Xuan Shen, Zhao Song, Yufa Zhou, Bo Chen, Jing Liu, Ruiyi Zhang, Ryan A. Rossi, Hao Tan, Tong Yu, Xiang Chen, Yufan Zhou, Tong Sun, Pu Zhao, Yanzhi Wang, and Jiuxiang Gu. Numerical pruning for efficient autoregressive models. In *Proceedings of the AAAI Conference on Artificial Intelligence*, 2025.
- [TJY⁺24] Keyu Tian, Yi Jiang, Zehuan Yuan, Bingyue Peng, and Liwei Wang. Visual autoregressive modeling: Scalable image generation via next-scale prediction. *Advances in neural information processing systems*, 2024.
- [Vil08] Cedric Villani. *Optimal transport: old and new*. Springer, 2008.
- [VSP⁺17] Ashish Vaswani, Noam Shazeer, Niki Parmar, Jakob Uszkoreit, Llion Jones, Aidan N Gomez, Łukasz Kaiser, and Illia Polosukhin. Attention is all you need. In *Advances in neural information processing systems*, pages 5998–6008, 2017.
- [WCY⁺23] Yuntao Wang, Zirui Cheng, Xin Yi, Yan Kong, Xueyang Wang, Xuhai Xu, Yukang Yan, Chun Yu, Shwetak Patel, and Yuanchun Shi. Modeling the trade-off of privacy preservation and activity recognition on low-resolution images. In *Proceedings of the 2023 CHI Conference on Human Factors in Computing Systems*, pages 1–15, 2023.

- [WCZ⁺23] Yilin Wang, Zeyuan Chen, Liangjun Zhong, Zheng Ding, Zhizhou Sha, and Zhuowen Tu. Dolfn: Diffusion layout transformers without autoencoder. *arXiv preprint arXiv:2310.16305*, 2023.
- [WXZ⁺24] Yilin Wang, Haiyang Xu, Xiang Zhang, Zeyuan Chen, Zhizhou Sha, Zirui Wang, and Zhuowen Tu. Omnicontrolnet: Dual-stage integration for conditional image generation. In *Proceedings of the IEEE/CVF Conference on Computer Vision and Pattern Recognition*, pages 7436–7448, 2024.
- [XLC⁺24] Haiyang Xu, Yu Lei, Zeyuan Chen, Xiang Zhang, Yue Zhao, Yilin Wang, and Zhuowen Tu. Bayesian diffusion models for 3d shape reconstruction. In *Proceedings of the IEEE/CVF Conference on Computer Vision and Pattern Recognition*, pages 10628–10638, 2024.
- [YLP⁺24] Hanshu Yan, Xingchao Liu, Jiachun Pan, Jun Hao Liew, Qiang Liu, and Jiashi Feng. Perflow: Piecewise rectified flow as universal plug-and-play accelerator. *arXiv preprint arXiv:2405.07510*, 2024.
- [ZCWT23] Xiang Zhang, Zeyuan Chen, Fangyin Wei, and Zhuowen Tu. Uni-3d: A universal model for panoptic 3d scene reconstruction. In *Proceedings of the IEEE/CVF International Conference on Computer Vision*, pages 9256–9266, 2023.
- [ZLCZ23] Kaiwen Zheng, Cheng Lu, Jianfei Chen, and Jun Zhu. Improved techniques for maximum likelihood estimation for diffusion odes. In *International Conference on Machine Learning*, pages 42363–42389. PMLR, 2023.
- [ZLKE23] Linqi Zhou, Aaron Lou, Samar Khanna, and Stefano Ermon. Denoising diffusion bridge models. *arXiv preprint arXiv:2309.16948*, 2023.

Appendix

Roadmap. In Section A, we provide a formal version of theoretical analysis and proofs.

A Theoretical Analysis

In this section, we first provide the formal theorem and proof for the sampling ODE in Section A.1. Then, we formally proved the speed limit of ForM's sampling ODE in Section A.2. In Section A.3, we formally prove the derivation of the interpolation path of ForM with TrigFlow. Last, we illustrate the formal proof for relativistic force in Section A.4.

A.1 Sampling ODE

Here, we restate the Theorem 4.2 and state its proof.

Theorem A.1 (Sampling ODE, formal version of Theorem 4.2). *Giving the force at position x_t denoted as $f_t(x_t)$, we could solve for ForM sampling path x_t by the following ODE*

$$\ddot{x}_t = \frac{1}{m^{\text{lab}}\gamma_t} (f_t^{\text{local}} - \frac{\langle v_t^{\text{lab}}, f_t^{\text{local}} \rangle}{c^2} v_t^{\text{lab}})$$

where $x_0 \sim \mathcal{N}(0, I)$, $\dot{x}_0 = 0$.

Proof. Recall f^{local} from Lemma A.5

$$f_t^{\text{local}} = m^{\text{lab}}(\gamma_t a_t^{\text{lab}} + \gamma_t^3 \frac{\langle v_t^{\text{lab}}, a_t^{\text{lab}} \rangle}{c^2} v_t^{\text{lab}}),$$

where γ_t is the Lorentz factor defined in Definition 3.1.

To solve for a_t^{lab} , we could first decompose a_t^{lab} by

$$a_t^{\text{lab}} = a_{t,\parallel}^{\text{lab}} + a_{t,\perp}^{\text{lab}},$$

where $a_{t,\parallel}^{\text{lab}}$ denotes the component of a_t^{lab} parallel with v_t^{lab} , and $a_{t,\perp}^{\text{lab}}$ denotes the component of a_t^{lab} perpendicular with v_t^{lab} .

According to the definition of parallel and perpendicular, we have

$$\begin{aligned} a_{t,\parallel}^{\text{lab}} &= \frac{\langle v_t^{\text{lab}}, a_t^{\text{lab}} \rangle}{\|v_t^{\text{lab}}\|_2^2} v_t^{\text{lab}}, \\ a_{t,\perp}^{\text{lab}} &= a_t^{\text{lab}} - a_{t,\parallel}^{\text{lab}}. \end{aligned}$$

Then we have

$$\begin{aligned} f_t^{\text{local}} &= m^{\text{lab}}(\gamma_t a_t^{\text{lab}} + \gamma_t^3 \frac{\langle v_t^{\text{lab}}, a_t^{\text{lab}} \rangle}{c^2} v_t^{\text{lab}}) \\ &= m^{\text{lab}}(\gamma_t (a_{t,\parallel}^{\text{lab}} + a_{t,\perp}^{\text{lab}}) + \gamma_t^3 \frac{\langle v_t^{\text{lab}}, a_{t,\parallel}^{\text{lab}} + a_{t,\perp}^{\text{lab}} \rangle}{c^2} v_t^{\text{lab}}) \\ &= m^{\text{lab}}(\gamma_t (a_{t,\parallel}^{\text{lab}} + a_{t,\perp}^{\text{lab}}) + \gamma_t^3 \frac{\langle v_t^{\text{lab}}, a_{t,\parallel}^{\text{lab}} \rangle}{c^2} v_t^{\text{lab}}), \end{aligned} \tag{3}$$

where the first step follows Lemma A.5, the second step decomposes a_t^{lab} , and the last step follows from the simple fact that $\langle v_t^{\text{lab}}, a_{t,\perp}^{\text{lab}} \rangle = 0$.

Then we decompose the f_t^{local} to $f_{t,\parallel}^{\text{local}}$ and $f_{t,\perp}^{\text{local}}$, where $f_{t,\parallel}^{\text{local}}$ denotes the component of f_t^{local} parallel with v_t^{lab} , and $f_{t,\perp}^{\text{local}}$ denotes the component of f_t^{local} perpendicular with v_t^{lab} .

For the perpendicular component, we have

$$\begin{aligned} f_{t,\perp}^{\text{local}} &= m^{\text{lab}} \gamma_t a_{t,\perp}^{\text{lab}} \\ a_{t,\perp}^{\text{lab}} &= \frac{f_{t,\perp}^{\text{local}}}{m^{\text{lab}} \gamma_t}, \end{aligned}$$

where the first step uses the perpendicular part from Eq. 3, and the second step rewrites the equation to get a closed-form solution for $a_{t,\perp}^{\text{lab}}$.

For the parallel component, we have

$$\begin{aligned} f_{t,\parallel}^{\text{local}} &= m^{\text{lab}} \left(\gamma_t a_{t,\parallel}^{\text{lab}} + \gamma_t^3 a_{t,\parallel}^{\text{lab}} \frac{\|v_t^{\text{lab}}\|_2^2}{c^2} \right) \\ &= m^{\text{lab}} a_{t,\parallel}^{\text{lab}} \left(\gamma_t + \gamma_t^3 \frac{\|v_t^{\text{lab}}\|_2^2}{c^2} \right) \\ a_{t,\parallel}^{\text{lab}} &= \frac{f_{t,\parallel}^{\text{local}}}{m^{\text{lab}} \left(\gamma_t + \gamma_t^3 \frac{\|v_t^{\text{lab}}\|_2^2}{c^2} \right)}, \end{aligned}$$

where the first step uses the parallel part from Eq. 3, the second step factors out the $a_{t,\parallel}^{\text{lab}}$, and the last step rewrites the equation to get a closed-form solution for $a_{t,\parallel}^{\text{lab}}$.

Then, we can combine these two components

$$\begin{aligned} a_t^{\text{lab}} &= \frac{f_{t,\perp}^{\text{local}}}{m^{\text{lab}} \gamma_t} + \frac{f_{t,\parallel}^{\text{local}}}{m^{\text{lab}} \left(\gamma_t + \gamma_t^3 \frac{\|v_t^{\text{lab}}\|_2^2}{c^2} \right)} \\ &= \frac{f_t^{\text{local}} - \frac{\langle v_t^{\text{lab}}, f_t^{\text{local}} \rangle}{\|v_t^{\text{lab}}\|_2^2} v_t^{\text{lab}}}{m^{\text{lab}} \gamma_t} + \frac{\frac{\langle v_t^{\text{lab}}, f_t^{\text{local}} \rangle}{\|v_t^{\text{lab}}\|_2^2} v_t^{\text{lab}}}{m^{\text{lab}} \left(\gamma_t + \gamma_t^3 \frac{\|v_t^{\text{lab}}\|_2^2}{c^2} \right)} \\ &= \frac{1}{m^{\text{lab}} \gamma_t} f_t^{\text{local}} + \frac{1}{m^{\text{lab}}} \left(\frac{1}{\gamma_t \left(1 + \gamma_t^2 \frac{\|v_t^{\text{lab}}\|_2^2}{c^2} \right)} - \frac{1}{\gamma_t} \right) \frac{\langle v_t^{\text{lab}}, f_t^{\text{local}} \rangle}{\|v_t^{\text{lab}}\|_2^2} v_t^{\text{lab}} \\ &= \frac{1}{m^{\text{lab}} \gamma_t} f_t^{\text{local}} + \frac{1}{m^{\text{lab}}} \left(\frac{1}{\gamma_t \frac{c^2}{c^2 - \|v_t^{\text{lab}}\|_2^2}} - \frac{1}{\gamma_t} \right) \frac{\langle v_t^{\text{lab}}, f_t^{\text{local}} \rangle}{\|v_t^{\text{lab}}\|_2^2} v_t^{\text{lab}} \\ &= \frac{1}{m^{\text{lab}} \gamma_t} f_t^{\text{local}} + \frac{1}{m^{\text{lab}}} \left(\frac{c^2 - \|v_t^{\text{lab}}\|_2^2}{\gamma_t c^2} - \frac{1}{\gamma_t} \right) \frac{\langle v_t^{\text{lab}}, f_t^{\text{local}} \rangle}{\|v_t^{\text{lab}}\|_2^2} v_t^{\text{lab}} \\ &= \frac{1}{m^{\text{lab}} \gamma_t} f_t^{\text{local}} - \frac{1}{m^{\text{lab}} \gamma_t} \frac{\|v_t^{\text{lab}}\|_2^2}{c^2} \frac{\langle v_t^{\text{lab}}, f_t^{\text{local}} \rangle}{\|v_t^{\text{lab}}\|_2^2} v_t^{\text{lab}} \\ &= \frac{1}{m^{\text{lab}} \gamma_t} \left(f_t^{\text{local}} - \frac{\langle v_t^{\text{lab}}, f_t^{\text{local}} \rangle}{c^2} v_t^{\text{lab}} \right), \end{aligned}$$

where the first step combines the two terms, the second step decomposes the components, the third step factors out the γ_t in denominator, the fourth uses the fact that $\gamma_t^2 = \frac{1}{1 - \|v_t^{\text{lab}}\|_2^2/c^2}$, the fifth step moves the denominator into numerator, the sixth step merges two terms, and the last step factors out the $\frac{1}{m^{\text{lab}} \gamma_t}$. \square

A.2 Speed Limit

In this subsection, we first calculate the derivative of the squared norm of velocity, then restate the Theorem 4.3 and provide its proof.

Lemma A.2 (Derivative of the squared norm of velocity). *Let $X(t) := \frac{1}{2}\|v_t^{\text{lab}}\|_2^2$. Then we have*

$$\frac{dX(t)}{dt} = \frac{\langle f_t^{\text{local}}, v_t^{\text{lab}} \rangle}{m^{\text{lab}}\gamma_t} \left(1 - \frac{\|v_t^{\text{lab}}\|_2^2}{c^2}\right).$$

Proof. Recall the sampling ODE

$$a_t^{\text{lab}} = \frac{1}{m^{\text{lab}}\gamma_t} \left(f_t^{\text{local}} - \frac{\langle v_t^{\text{lab}}, f_t^{\text{local}} \rangle}{c^2} v_t^{\text{lab}} \right), \quad (4)$$

where γ_t is the Lorentz factor at lab time t defined in Definition 3.1.

We can show that

$$\begin{aligned} \frac{dX(t)}{dt} &= \frac{d}{dt} \frac{1}{2} \|v_t^{\text{lab}}\|_2^2 \\ &= \left\langle v_t^{\text{lab}}, \frac{d}{dt} v_t^{\text{lab}} \right\rangle \\ &= \langle v_t^{\text{lab}}, a_t^{\text{lab}} \rangle \\ &= \left\langle v_t^{\text{lab}}, \frac{1}{m^{\text{lab}}\gamma_t} \left(f_t^{\text{local}} - \frac{\langle v_t^{\text{lab}}, f_t^{\text{local}} \rangle}{c^2} v_t^{\text{lab}} \right) \right\rangle \\ &= \frac{1}{m^{\text{lab}}\gamma_t} \langle f_t^{\text{local}}, v_t^{\text{lab}} \rangle - \frac{\langle v_t^{\text{lab}}, f_t^{\text{local}} \rangle}{m^{\text{lab}}\gamma_t c^2} \|v_t^{\text{lab}}\|_2^2 \\ &= \frac{\langle f_t^{\text{local}}, v_t^{\text{lab}} \rangle}{m^{\text{lab}}\gamma_t} \left(1 - \frac{\|v_t^{\text{lab}}\|_2^2}{c^2}\right) \end{aligned}$$

where the first step follows from the definition of $X(t)$, the second step follows from the chain rule, the third step follows from the basic fact, the fourth step follows from the Eq. (4), the fifth and last step follows from basic algebra. \square

Here, we restate the Theorem 4.3 and state its proof.

Theorem A.3 (Speed Limit, formal version of Theorem 4.3). *For a ForM model with sampling path $x : [0, T) \rightarrow \mathbb{R}^n$, the velocity satisfies*

$$\|\dot{x}_t\|_2 < c \quad \text{for all } t \in [0, T).$$

Proof. Let $X(t) := \frac{1}{2}\|v_t^{\text{lab}}\|_2^2$. By Lemma A.2, we have

$$\frac{dX(t)}{dt} = \frac{1}{m^{\text{lab}}\gamma_t} \langle f_t^{\text{local}}, v_t^{\text{lab}} \rangle \left(1 - \frac{\|v_t^{\text{lab}}\|_2^2}{c^2}\right).$$

Observe that the factor $(1 - \|v_t^{\text{lab}}\|_2^2/c^2)$ becomes negative if ever $\|v_t^{\text{lab}}\|_2 > c$, and it is zero when $\|v_t^{\text{lab}}\|_2 = c$. Thus, if the velocity norm were to exceed c at some time, the derivative of $X(t)$ at that moment would be negative, forcing $X(t)$ (i.e., $\|v_t^{\text{lab}}\|_2^2$) to decrease rather than increase. In particular, once $\|v_t^{\text{lab}}\|_2^2$ reaches c^2 , it cannot increase further.

Consequently, for all $t \in [0, T)$ we must have $\|v_t^{\text{lab}}\|_2 < c$, which proves the speed limit. Equivalently, since $\dot{x}_t = v_t^{\text{lab}}$ in our notation, we conclude

$$\|\dot{x}_t\|_2 < c, \quad \forall t \in [0, T).$$

Thus, we complete the proof. \square

A.3 ForM with TrigFlow

We restate the Theorem 4.4 and provide its proof.

Theorem A.4 (ForM with TrigFlow, formal version of Theorem 4.4). *We let $m = 1$ for simplicity in ForM. Giving a the interpolation $x_t = \alpha_t x_1 + \sigma_t x_0$, where $\alpha_T = 1$, $\alpha_0 = 0$, $\sigma_T = 0$, $\sigma_0 = 1$. We let $F_t(x_t)$ denote a vector map of force, a trainable neuron network parameterized with θ . We select the α_t and σ_t identical with TrigFlow [LS24], where $\alpha_t = \sin(t)$ and $\sigma_t = \cos(t)$, $T = \frac{\pi}{2}$. Then, force interpolation could be simplified to*

$$f_t(x_t) = \frac{(\cos(t)x_1 - \sin(t)x_0) \cdot (-\sin(t)x_1 - \cos(t)x_0)}{c^2 - (\cos(t)x_1 - \sin(t)x_0)^2} (\cos(t)x_1 - \sin(t)x_0).$$

Proof. We can show that

$$\begin{aligned} f_t(x_t) &= \gamma_t \ddot{x}_t + \gamma_t^3 \frac{\langle \dot{x}_t, \ddot{x}_t \rangle}{c^2} \dot{x}_t \\ &= \left(1 - \frac{(\cos(t)x_1 - \sin(t)x_0)^2}{c^2}\right)^{-\frac{1}{2}} (-\sin(t)x_1 - \cos(t)x_0) + \\ &\quad \frac{(\cos(t)x_1 - \sin(t)x_0) \cdot (-\sin(t)x_1 - \cos(t)x_0)}{c^2 - (\cos(t)x_1 - \sin(t)x_0)^2} \\ &\quad (\cos(t)x_1 - \sin(t)x_0), \end{aligned}$$

where we use Definition 3.3 and substitute acceleration a_t^{lab} with \ddot{x}_t and v_t^{lab} with \dot{x}_t in the first step, and substitute $x_t = \sin(t)x_1 + \cos(t)x_0$ and calculate it's derivative in the second step. \square

A.4 Relativistic Force Property

In this subsection, we restate Lemma 3.4, and show its proof.

Lemma A.5 (Equivalent Form of Relativistic Force, formal version of Lemma 3.4). *Let p^{lab} be the momentum defined in Eq. (2), γ_t be the Lorentz factor at lab time t defined in Definition 3.1, τ denotes the proper time, $v_t^{\text{lab}} = \dot{x}_t$ denotes the velocity, $a_t^{\text{lab}} = \ddot{x}_t$ denotes the acceleration. The relativistic force, defined as the time derivative of the momentum in the lab frame, can be written as*

$$f^{\text{local}} = m^{\text{lab}} (\gamma_t a_t^{\text{lab}} + \gamma_t^3 \frac{\langle v_t^{\text{lab}}, a_t^{\text{lab}} \rangle}{c^2} v_t^{\text{lab}}).$$

Proof. We can show that

$$\begin{aligned} f^{\text{local}} &= \frac{dp^{\text{lab}}}{d\tau} \\ &= \frac{dm^{\text{lab}} v_t^{\text{lab}} \gamma_t}{dt} \\ &= m^{\text{lab}} \frac{dv_t^{\text{lab}} \gamma_t}{dt} \\ &= m^{\text{lab}} (\gamma_t a_t^{\text{lab}} + \gamma_t^3 \frac{\langle v_t^{\text{lab}}, a_t^{\text{lab}} \rangle}{c^2} v_t^{\text{lab}}). \end{aligned}$$

where the first step follows from Eq. (1), the second step follows Eq. (2) and Definition 3.2, the third step is true because m^{lab} is a constant, and the last step takes the derivative. \square